Magnetomechanical Multiscale Hysteresis Model of Electrical Steel Sheets in the Finite Element Simulation of a Transformer

F. Martin[1], J. Taurines[1,2], O. Osemwinyen[1], P. Rasilo[2], A. Belahcen[1], and L. Daniel[3,4]

[1]Department of Electrical Engineering and Automation, Aalto University, FI-00076 Aalto, Finland
[2]Electrical Engineering Unit, Tampere University, Tampere University, FI-33014 Tampere, Finland
[3]CentraleSupélec, CNRS, Laboratoire de Génie électrique et électronique de Paris, Université Paris-Saclay, 91192 Gif-sur-Yvette, France
[4]CNRS, Laboratoire de Génie électrique et électronique de Paris, Sorbonne Université, 75252 Paris, France

In this article, a multiscale model incorporates an energy-based hysteresis model for ferromagnetic material. The coherent rotational phenomena are considered by letting the magnetic domains rotate with the applied field. Hence, the drop of the hysteresis losses under increasing rotational flux density can be modeled properly without any additional artifacts. The model parameters are identified from a microstructure X-ray analysis and a standard unidirectional magnetic characterization. The material behavior is validated under various magnetomechanical loadings. Finally, the multiscale hysteresis model is deployed within a finite element analysis of a transformer. The model can properly predict the measured flux-density waveform under quasistatic condition.

***Index Terms*— Finite element analysis, magnetomechanical effects, multidimensional systems, soft magnetic material.**

I. Introduction

THE analysis and the design of electrical applications play important roles in the energy transition, pushing forward the electric mobility and sustainable energy production. In this context, the accurate prediction of the simulated system losses can appropriately adjust the design of the application toward efficient and reliable systems. The magnetomechanical phenomena in electrical steel sheets tend to degrade the performance of electrical applications. The mechanical deformation is exerted in the steel as an elastic strain to maintain the components in place [1], [2], [3], [4] but also as a plastic deformation due to the cutting process of the steel sheets into the desired shape [5], [6], [7], [8]. The magnetomechanical loading of an electric application over its lifetime requires developing simulation models, which retain high accuracy in the extrapolation range, i.e., outside the scope of the identification dataset. Among the different magnetomechanical models of electric steel sheets, the multiscale model [1], [3], [4], [9] can properly predict the material behavior under various multiaxial magnetoelastic loadings. In [9], the multiscale model is introduced for the anhysteretic behavior of electrical steel sheets. The consideration of the material texture enables the prediction of the anisotropic properties. In [1], the Jiles–Atherton model is incorporated into the multiscale model for evaluating the performance of a switched reluctance motor. Although the texture is simplified and limited to a single grain equivalent to an isotropic texture, the multiscale model is efficiently incorporated in a finite element method. In [3], the anhysteretic multiscale model is implemented into a finite element method for a realistic texture composed of 396 grains.

In this article, we propose to implement the energy-based hysteresis model [10] in the multiscale magnetomechanical model. The coherent rotation of the domain is naturally represented by letting the magnetization orientations of the domains rotate when the domain walls are pinned. The impact of the stress on the strength of the pinning sites can be predicted from the coercive field theory [11]. Hence, the material parameters can be identified with a standard single sheet tester. The material behavior is validated under various multiaxial mechanical loadings under rotational and alternating flux-density conditions. Finally, the multiscale hysteresis model is implemented into the finite element simulation of a transformer. The measured flux-density waveform is properly predicted by the model.

Manuscript received 13 June 2024; revised 19 August 2024; accepted 19 August 2024. Date of publication 22 August 2024; date of current version 26 November 2024. Corresponding author: F. Martin (e-mail: floran.martin@aalto.fi).

Color versions of one or more figures in this article are available at https://doi.org/10.1109/TMAG.2024.3448228.

Digital Object Identifier 10.1109/TMAG.2024.3448228

II. Model

A. Multiscale Anhysteretic Magnetoelastic Model

The anhysteretic behavior of electrical steel is modeled with the multiscale model presented in [3] and [9]. The applied magnetic field $\boldsymbol{h}_e$ and mechanical stress $\boldsymbol{\sigma}_e$ are first localized into a grain g with a self-consistent scheme [9]. The mesoscopic magnetomechanical loadings $\boldsymbol{h}_g$ and $\boldsymbol{\sigma}_g$ affect both the magnetization orientation and the volume fraction of the magnetic domains. The magnetization orientations $\boldsymbol{e}_i$ of the six domain types are evaluated by minimizing the free Gibbs energy W_g with respect to the magnetization orientation $\boldsymbol{e}$. Expressed in the crystal frame, it is given by

$$W_g(\boldsymbol{e}) = W_{\text{an}}(\boldsymbol{e}) - \mu_0 M_s \boldsymbol{h}_g \cdot \boldsymbol{e} - \boldsymbol{\sigma}_g : \boldsymbol{\varepsilon}_\mu(\boldsymbol{e}) \tag{1}$$

where μ_0 is the vacuum permeability and M_s is the saturation magnetization. The magnetostriction is given as in [3] and [9] by

$$\boldsymbol{\varepsilon}_\mu = \frac{3}{2}\lambda_{100}\left[(\boldsymbol{e}\otimes\boldsymbol{e})\odot\mathbf{I} - \frac{1}{3}\mathbf{I}\right] + \frac{3}{2}\lambda_{111}(\boldsymbol{e}\otimes\boldsymbol{e})\odot\bar{\mathbf{I}} \tag{2}$$

where λ_{100} and λ_{111} are the magnetostriction saturation constants. $\mathbf{I}$ is the identity matrix, and $\bar{\mathbf{I}}$ is defined, so that $\mathbf{I}+\bar{\mathbf{I}}$ is a matrix full of 1. $\odot$ is the Hadamard product. The term 1/3 ensures the isochoric property of the magnetostriction. W_{an}

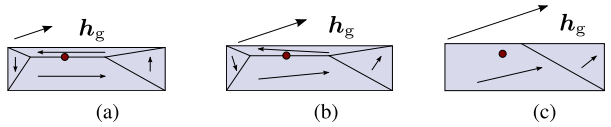

Fig. 1. Synoptic of the coherent rotation of the domain. (a) Field is too small to unpin the domain wall from the defect, and the magnetocrystalline anisotropic energy is dominant, letting the magnetization orientation near the easy axis. (b) Field is large enough to initiate the rotation of the magnetic domains, but it is too low for unpinning the magnetic wall from the defect. (c) Large field unpins the domain wall from the defect, and the magnetic domains align further toward the field direction.

is the magnetocrystalline anisotropy energy defined as in [3] and [9]

$$W_{\text{an}} = \frac{K_1}{2}\left[(\boldsymbol{e}\otimes\boldsymbol{e})\odot\bar{\mathbf{I}}\right] : \left[(\boldsymbol{e}\otimes\boldsymbol{e})\odot\bar{\mathbf{I}}\right] \tag{3}$$

where K_1 is the first magnetocrystalline anisotropy constant.

The domain volume fraction v_i is evaluated by maximizing the statistical entropy of the magnetic domains, distinct by their energy $W_i = W_g(\boldsymbol{e}_i)$. This leads to the following Boltzmann distribution:

$$v_i = \frac{\exp(-A_0 W_i)}{\sum_{i=1}^{6}\exp(-A_0 W_i)} \tag{4}$$

where $A_0 = 3\chi_0/(\mu_0 M_s^2)$ is a material constant, which depends on the initial energy state of the crystal [7], [8]. χ_0 is the initial susceptibility of the anhysteretic magnetization.

The magnetization, the magnetostriction, and the mesoscopic energy of a grain are determined by the sum of the magnetic domain properties weighted by the volume fraction of the magnetic domains. The macroscopic response of the material is calculated following a homogenization process [9].

B. Energy-Based Hysteresis Model

The energy-based hysteresis model decomposes the magnetic field into a reversible $\boldsymbol{h}_r$ and an irreversible part $\boldsymbol{h}_i$ [10]. At the mesoscopic scale, it leads to $\boldsymbol{h}_g = \boldsymbol{h}_r + \boldsymbol{h}_i$. The irreversible field represents the pinning of the domain wall to defects as a magnetic strength to keep the domain wall in position and maintain the domain volume fraction. Multiple hysterons, N_{hyst}, account for the large diversity of the pinning sites with different amplitudes of the magnetic strength κ_j. The reversible field of the hysteron j is computed by

$$\boldsymbol{h}_{r_j} = \left[\boldsymbol{h}_g - \kappa_j \frac{\boldsymbol{h}_g - \boldsymbol{h}_{ro_j}}{\|\boldsymbol{h}_g - \boldsymbol{h}_{ro_j}\|}\right]\delta_j + (1-\delta_j)\boldsymbol{h}_{ro_j} \tag{5}$$

where δ_j is the Boolean value of the inequality $\|\boldsymbol{h}_g - \boldsymbol{h}_{ro_j}\| > \kappa_j$. $\boldsymbol{h}_{ro_j}$ is the reversible field of the hysteron j at the previous loading level. The domain volume fraction (4) is evaluated with the crystal energy (1) by considering the reversible field $\boldsymbol{h}_{r_j}$ instead of the mesoscopic field $\boldsymbol{h}_g$. However, the magnetization orientations of the magnetic domains are determined with the mesoscopic field similar to the anhysteretic model. Indeed, the domain orientations represent the energy minima of the matter where the defects affect only a small portion of the soft ferromagnetic materials. Hence, we can neglect the localized defect energy while determining the energy minima, which lets the domain magnetization rotates even when the domain walls are pinned. This concept is illustrated in Fig. 1.

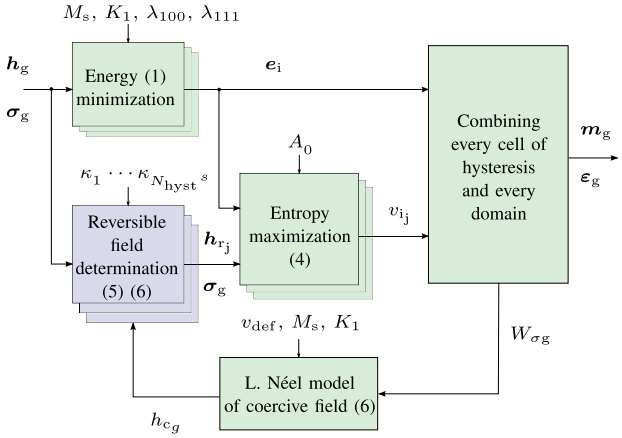

Fig. 2. Synoptic of the multiscale hysteresis model with the coherent rotation.

The application of a mechanical stress affects the coercive field. This phenomenon is considered by scaling the hysteron's magnetic strength κ_j with the relative variation of the coercive field due to the stress, $h_c(\sigma)/h_c(0)$. The impact of the stress on the coercive field is predicted from the coercive field theory of Néel [11]. It is based on the energetic equivalence between the magnetomechanical energy of the pinned domain wall and the stray field energy induced once the defect is left within a magnetic domain. The prediction of the coercive field depends on the volume fraction of the defects v_{def} and the mesoscopic magnetoelastic energy $W_{\sigma g}$ by

$$h_{c_g} = \frac{4P_c}{\pi\mu_0 M_s}\frac{W_{\sigma g}^2}{K_1 + r_c W_{\sigma g}}\left[\ln\sqrt{\frac{2\pi\mu_0^2 M_s^2}{K_1 + r_c W_{\sigma g}}} - 6.673\right] + \frac{2v_{\text{def}}K_1 M_s}{\pi\mu_0 M_s}\left[\ln\sqrt{\frac{2\pi\mu_0^2 M_s^2}{K_1}} - 7.673\right] \tag{6}$$

with $P_c = 1/15$ and $r_c = -2/7$ for iron-based material. The first term contains the influence of the magnetoelastic energy of a grain $W_{\sigma g} = -\sum_{i=1}^{6} v_i \boldsymbol{\sigma}_g : \boldsymbol{\varepsilon}_\mu(\boldsymbol{e}_i)$. The second term contains the influence of the impurities and initial micromechanical defects. We consider that interstitial atoms correspond to the defects of volume fraction v_{def}. In Fig. 2, the synoptic presents the implementation of the hysteresis model in the multiscale model for soft ferromagnetic materials.

C. Finite Element Method

The implementation of the multiscale hysteresis model in the finite element method is presented for the $\boldsymbol{t}-\phi$ formulation with the electric vector potential $\boldsymbol{t}$ and the magnetic scalar potential ϕ [13]. In the absence of eddy currents, the formulation for a non-linear material is defined in the bounded volume Ω without external flux source by

$$\begin{cases} \int_\Omega (\nabla\times\boldsymbol{t})\cdot\left(\nabla\times\boldsymbol{h}'_{\text{rot}}\right)\mathrm{d}v = \int_\Omega \boldsymbol{j}_s\cdot\nabla\times\boldsymbol{h}'_{\text{rot}}\,\mathrm{d}v \\ \int_\Omega \frac{\partial\boldsymbol{b}}{\partial\boldsymbol{h}}\boldsymbol{h}\cdot\nabla\phi'_{\text{irr}}\,\mathrm{d}v = \int_\Omega \boldsymbol{b}_{\text{nl}}\cdot\nabla\phi'_{\text{irr}}\,\mathrm{d}v \text{ with } \boldsymbol{h} = \boldsymbol{t} - \nabla\phi \end{cases} \tag{7}$$

where $\boldsymbol{h}'_{\text{rot}}$ and ϕ'_{irr} are the test functions of the electric vector potential and the magnetic scalar potential. $\boldsymbol{j}_s$ is the source current density. The Whitney–Nédélec elements of order 1 support the electric vector potential $\boldsymbol{t}$ along the cotree subset of

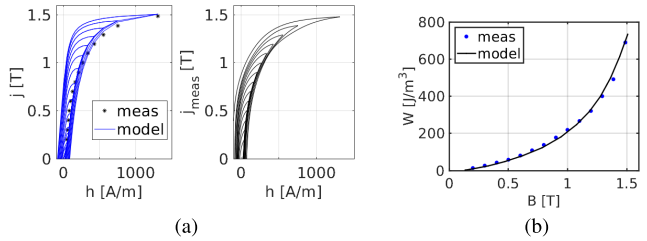

Fig. 3. Comparison between the model and the measurement along the TD for the identification procedure. In (a), the simulation of the first magnetization is compared with the measured peak of the symmetric loops. Measured and simulated symmetric loops are reported. (a) Polarization along TD. (b) Alternating loss along TD.

the mesh edges. The magnetic scalar potential ϕ is discretized with the Lagrangian elements of order 2 to remain consistent in the definition of $\boldsymbol{h}$. The term $\boldsymbol{b}_{\text{nl}}$ contains the source terms of the first-order approximation of $\boldsymbol{b}(\boldsymbol{h})$. It is given with the field $\boldsymbol{h}_0$ and the flux density $\boldsymbol{b}_0$ computed at the previous iteration by

$$\boldsymbol{b}_{\text{nl}} = \frac{\partial \boldsymbol{b}}{\partial \boldsymbol{h}} \boldsymbol{h}_0 - \boldsymbol{b}_0. \tag{8}$$

To improve the convergence rate, the Jacobian is modified by

$$\frac{\partial \boldsymbol{b}}{\partial \boldsymbol{h}} = \mu_0 \left[\mathbf{I} + r\chi_0 \mathbf{I} + (1-r)\frac{\partial \boldsymbol{m}}{\partial \boldsymbol{h}} \right]. \tag{9}$$

The term $\partial \boldsymbol{m}/\partial \boldsymbol{h}$ is computed by incorporating the hysteresis in the expression given in [3]. The solver parameter $r = 0.5$ gives the fastest convergence rate.

III. Results

A. Material Model

The parameters of the multiscale model are reported in [3] for an electrical steel sheet M400-50A with $FeSi_{3\%}$. The volume fraction of the defects is assumed to be the same as the volume fraction of the chemical impurities, which appear in the single crystal as interstitial atoms. In our material, it corresponds to 0.1%. The intensity and the volume fraction of 20 hysterons are identified from stress-free magnetic measurements realized under alternating conditions at 10 Hz along the transverse direction (TD) in a rotational single sheet tester, reported in [14]. The hysteresis parameters are determined to minimize the sum of the squares of the errors between the tips of the measured BH loops and the model of the first magnetization. In Fig. 3, the measured BH loops and the hysteresis loss can be accurately estimated with the multiscale hysteresis model on the identification set.

In Fig. 4(a), the model is validated under rotational flux-density conditions. By employing the modified Jacobian, the Newton–Raphson method is deployed to simulate the rotational flux-density condition with the multiscale hysteresis model. The proposed model of the coherent rotation can properly predict the measured loss as well as extrapolate the losses with a peak of loss for a rotational flux density with an amplitude of 1.48 T. Neglecting the localized energy of the defect is justified, especially with the small defect volume fraction. In Fig. 4(b), the loci of the magnetic fields are compared in the case of uniaxial compressive stress applied along

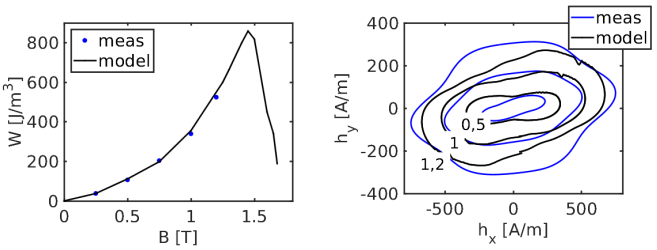

Fig. 4. Model validation under rotational flux-density condition. The in-plane stress is given in the following notation [$\sigma_{\text{RD RD}}$; $\sigma_{\text{TD TD}}$; $\sigma_{\text{RD TD}}$]. (a) Without stress. (b) $\boldsymbol{\sigma} = [-30$ MPa; 0; 0].

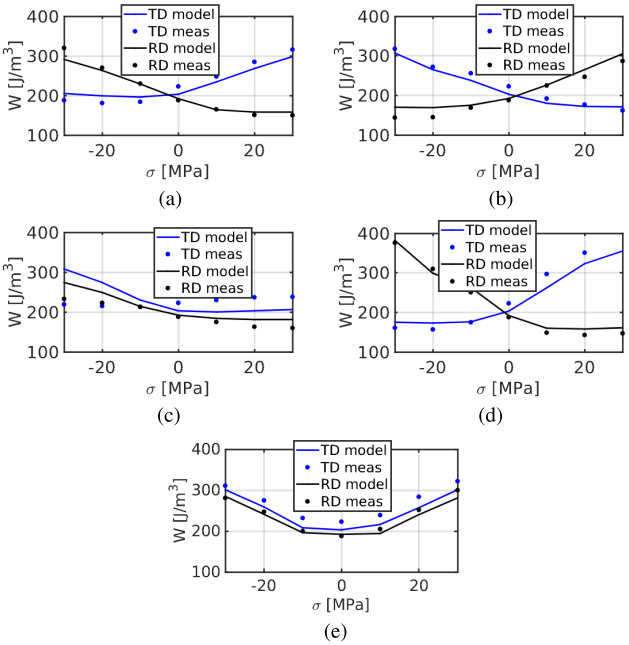

Fig. 5. Model validation under different static mechanical loadings and alternating flux conditions at 1 T, 10 Hz. The in-plane stress is given in the following notation [$\sigma_{\text{RD RD}}$; $\sigma_{\text{TD TD}}$; $\sigma_{\text{RD TD}}$]. (a) $\boldsymbol{\sigma} = [\sigma; 0; 0]$. (b) $\boldsymbol{\sigma} = [0; \sigma; 0]$. (c) $\boldsymbol{\sigma} = [\sigma; \sigma; 0]$. (d) $\boldsymbol{\sigma} = [\sigma; -\sigma; 0]$. (e) $\boldsymbol{\sigma} = [0; 0; \sigma]$.

the rolling direction (RD). Although some discrepancies can be noted, the model is properly able to predict the anisotropic behavior induced by both the stress and the material texture.

In Fig. 5, the multiscale hysteresis model is validated under multiple stress states, in the case of alternating magnetic flux density applied along the rolling and the TDs. The flux-density amplitude is kept at 1 T for the simulation and the measurement. In Fig. 5(a) and (b), the application of a uniaxial stress and a magnetic flux density along the same direction and the orthogonal direction are quasi-symmetric, as observed in [14]. The application of a biaxial stress [Fig. 5(c)] presents the largest predictive error of 30%. Nevertheless, even in this condition, the trend of the loss is properly assessed. Both the pseudo-shear and the pure-shear cases are accurately represented with the multiscale hysteresis model. The variation of the losses in the case of a pure shear stress loading [Fig. 5(e)] presents a similar level as the uniaxial loadings. Although the equivalent macroscopic isotropic magnetostriction [15] could be deployed to simplify the multiscale model, the vanishing magnetostriction shear would mask the effect of the shear stress. Including the grain scale can capture this effect.

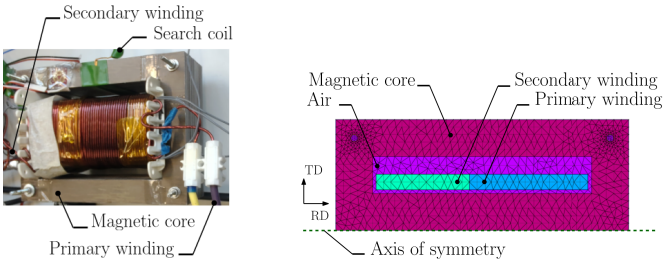

Fig. 6. Transformer nomenclature and 2-D mesh discretization. (a) Nomenclature. (b) Mesh and domains.

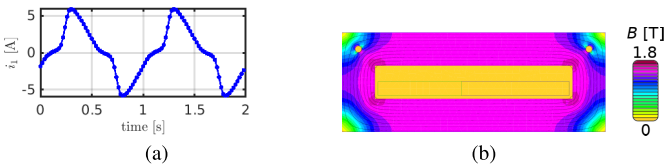

Fig. 7. Measured and applied current waveform and simulated flux-density amplitude at the current peak. The applied voltage is sinusoidal. (a) Applied current. (b) Flux-density distribution.

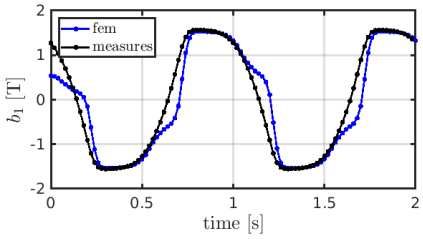

Fig. 8. Comparison between the flux-density waveform measured by the search coil and the simulated by the finite element model with the multiscale hysteresis model.

B. Application to a Transformer

The multiscale hysteresis model is employed to simulate the magnetic core of a 120-mm-long transformer with FreeFem++ [16]. The magnetic core is composed of 80 sheets of 15-mm width, represented in Fig. 6. Since the applied field remains in the orthotropic plane of symmetry of the material, the simulation can be conducted in 2-D. The measured current waveform is applied in the primary coil of the transformer to reproduce the open-circuit operation [Fig. 7(a)]. In Fig. 7(b), the flux-density distribution is represented when the current is maximal. The flux density approaches the saturation in the inner corners and near the non-magnetic screws. In Fig. 8, the measured flux density can be properly evaluated by the finite element method. Although some discrepancies can be noted at low flux-density level, the multiscale model can reproduce the peak of the flux density accurately. The discrepancies may come from the non-homogeneity of the magnetic quantities and the demagnetization effect of the rotational single sheet tester [14]. Furthermore, the effect of the deterioration due to the punching of the transformer lamination may affect the magnetic properties [5], [6].

IV. Conclusion

In this article, we implement an energy-based hysteresis model into a multiscale magnetomechanical model. The domain volume fraction is adjusted by the reversible field, whereas the magnetization orientations of the domains are computed by minimizing the energy by neglecting the pinning site energy. Hence, the coherent rotation of the magnetic domains is properly represented without any additional parameters. Because of the coercive field theory [11], the hysteresis parameters are identified under standard stress-free magnetic characterization. The model is validated under various alternating and rotational magnetomechanical loadings. Finally, the multiscale hysteresis model is implemented into a finite element method for simulating a transformer. Although some discrepancies can be noticed at low flux-density level, the flux-density peak is accurately reproduced by the suggested model.

Acknowledgment

The work of F. Martin, J. Taurines, A. Belahcen, and P. Rasilo was supported by the Research Council of Finland through the Centre of Excellence in High-Speed Electromechanical Energy Conversion Systems under Grant 346438.

References

[1] L. Bernard and L. Daniel, "Effect of stress on magnetic hysteresis losses in a switched reluctance motor: Application to stator and rotor shrink fitting," *IEEE Trans. Magn.*, vol. 51, no. 9, pp. 1–13, Sep. 2015.

[2] K. Yamazaki, Y. Sato, M. Domenjoud, and L. Daniel, "Iron loss analysis of permanent-magnet machines by considering hysteresis loops affected by multi-axial stress," *IEEE Trans. Magn.*, vol. 56, no. 1, pp. 1–4, Jan. 2020.

[3] F. Martin et al., "Analysis of the magneto-mechanical anisotropy of steel sheets in electrical applications," *IEEE Trans. Magn.*, vol. 56, no. 2, pp. 1–4, Feb. 2020.

[4] L. G. da Silva, L. Bernard, F. Martin, A. Belahcen, and L. Daniel, "Multiaxial validation of a magneto-elastic vector-play model," *IEEE Trans. Magn.*, vol. 59, no. 11, pp. 1–10, Nov. 2023.

[5] N. M'zali, F. Martin, U. Aydin, A. Belahcen, A. Benabou, and T. Henneron, "Determination of stress dependent magnetostriction from a macroscopic magneto-mechanical model and experimental magnetization curves," *J. Magn. Magn. Mater.*, vol. 500, Apr. 2020, Art. no. 166299.

[6] I. T. Gürbüz, F. Martin, P. Rasilo, M. M. Billah, and A. Belahcen, "A new methodology for incorporating the cutting deterioration of electrical sheets into electromagnetic finite-element simulation," *J. Magn. Magn. Mater.*, vol. 593, Mar. 2024, Art. no. 171843.

[7] M. Domenjoud and L. Daniel, "Effects of plastic strain and reloading stress on the magneto-mechanical behavior of electrical steels: Experiments and modeling," *Mech. Mater.*, vol. 176, Jan. 2023, Art. no. 104510.

[8] J. Taurines, F. Martin, P. Rasilo, and A. Belahcen, "Thermodynamic description for magneto-plastic coupling in electrical steel sheets," *J. Magn. Magn. Mater.*, vol. 593, Mar. 2024, Art. no. 171846.

[9] L. Daniel, O. Hubert, N. Buiron, and R. Billardon, "Reversible magneto-elastic behavior: A multiscale approach," *J. Mech. Phys. Solids*, vol. 56, no. 3, pp. 1018–1042, Mar. 2008.

[10] F. Henrotte et al., "An energybased vector hysteresis model for ferromagnetic materials," *COMPEL*, vol. 25, no. 1, pp. 71–80, 2006.

[11] L. Néel, "Bases d'une nouvelle théorie générale du champ coercitif," *Ann. Univ. Genoble*, vol. 22, pp. 299–343, Jan. 1946.

[12] R. Chen, F. Martin, Y. Li, S. Yue, and A. Belahcen, "An energy-based anisotropic vector hysteresis model for rotational electromagnetic core loss," *IEEE Trans. Ind. Electron.*, vol. 71, no. 6, pp. 6084–6094, Jun. 2024.

[13] T. Tarhasaari, A. Koski, K. Forsman, and L. Kettunen, "Hybrid formulations for eddy current problem with moving objects," *IEEE Trans. Magn.*, vol. 34, no. 5, pp. 2660–2663, Jan. 1998.

[14] U. Aydin et al., "Rotational single sheet tester for multiaxial magneto-mechanical effects in steel sheets," *IEEE Trans. Magn.*, vol. 55, no. 3, pp. 1–10, Mar. 2019.

[15] E. D. T. de Lacheisserie, *Magnetostriction Theory and Applications of Magnetoelasticity*. Boca Raton, FL, USA: CRC Press, Jun. 1993.

[16] F. Hecht, "New development in freefem++," *J. Numer. Math.*, vol. 20, nos. 3–4, pp. 251–266, Jan. 2012.